Numerical Diagnostic to Investigate Poloidal Asymmetry in Three-Dimensional Magnetic Configurations

N. Kasuya [1], M. Nunami [2], K. Tanaka [2], C. A. Michael [3], S. Toda [2] and M. Yagi [4]

[1] Research Institute for Applied Mechanics, Kyushu University, Kasuga, Fukuoka 816-8580, Japan

[2] National Institute for Fusion Science, Toki, Gifu 509-5292, Japan

[3] Plasma Research Laboratory, Australian National University, Canberra, A.C.T. 2601, Australia

[4] National Institute for Quantum and Radiological Science and Technology, Obuchi, Rokkasho, Aomori 039-3212, Japan

E-mail contact of main author: kasuya@riam.kyushu-u.ac.jp

Abstract. Several experimental observations show detailed distributions of plasma turbulence, which can affect plasma transport. Complicated configurations make it difficult to capture the entire structures of fluctuations in helical plasmas, so three-dimensional (3-D) turbulence simulations are necessary for identifying the characteristic features. We are developing the Turbulence Diagnostic Simulator (TDS), and carry out the numerical diagnostics in Large Helical Device (LHD) for that purpose. In this research, the gyrokinetic simulation code GKV-X provides turbulent fluctuations in 3-D configurations, and then, the TDS calculates its line-integration along the line of sight (LS) as in phase contrast imaging (PCI) to give numerical observation signals, and the pitch angle of the magnetic field is used to reconstruct a local spectrum with consideration of a spatial resolution. In the results of the synthetic diagnostic, three factors to induce the poloidal asymmetry of fluctuations are evaluated; (i) 3-D magnetic configuration with the realistic LS, (ii) effect of signal processing techniques, and (iii) inherent inhomogeneity of the turbulence itself. The original data includes only small up-down asymmetry, because this is given from an ion temperature gradient (ITG) turbulence simulation in a single flux-tube. The effects (i) and (iii) generate the asymmetry, which is sometimes enhanced by the effect (ii). The asymmetry is less than several tens of percent in this case as in the high ion temperature experiment with ITG excitation. These quantitative evaluations represent a guideline for comparison of observed signals from experiments and simulations.

1. Introduction

Turbulence measurements have suggested the importance of poloidal inhomogeneity in transport in torus plasmas [1]. In Large Helical Device (LHD) [2], profiles of the density fluctuations have been measured by the phase contrasting imaging (PCI) diagnostic [3],[4]. Complicated configurations make it difficult to capture the entire structures of fluctuations, so turbulence simulations in three-dimensional (3-D) magnetic configurations are necessary for interpretation of experimental observations in helical plasmas [5]-[8]. Synthetic diagnostics to simulate experimental measurements are effective for validation for the simulation result [9]-[12]. For a helical plasma, using the GKV-X [13],[14] which is a gyrokinetic Vlasov code with 3-D equilibrium in experimental magnetic configurations, quantitative comparisons with experiments have been carried out for the validation [14],[15]. Turbulence Diagnostic Simulator (TDS) [16] is a combination of turbulence codes, measurement modules and analysis routines, to carry out numerical experiments of plasma turbulence, which can be

utilized as a platform of the data analysis. Data from various simulations are analyzed with the routines to give diagnostics as in an actual experiment. Demonstration of the numerical PCI was carried out to give a fluctuation spectrum [15]. The simulations calculate ion-temperature-gradient (ITG) turbulence, and line-integration along the line of sight (LS) of the 3-D fluctuations as in PCI gives numerical observation signals. A spatial profile of the turbulence spectrum is reconstructed from the signals with finite resolution, which is compared with the experiment. The TDS is applied for the investigation of the up-down asymmetry here. (i) The 3-D magnetic configuration with the realistic LS induces a little asymmetry, which is enhanced by (ii) the effect of signal processing techniques in some cases. (iii) Inherent inhomogeneity of turbulence, calculated from the toroidal and poloidal dependency of the local ITG instabilities, also gives spatial variation of turbulent intensities. The up-down asymmetry of the fluctuation amplitudes is within several tens of percent, as the ITG observation in the LHD experiments.

2. Method

A numerical diagnostic to simulate an experimental measurement is carried out using gyrokinetic simulations of ITG modes in the LHD configuration. The effect of line integration along the LS is considered as in the PCI measurement. The observation is carried out with a limited number of detectors, and the signal processing techniques are applied to improve the spatial resolution of the spectrum.

2.1. Turbulence simulation

Flux-tube simulations of ITG modes in the LHD configuration have been carried out with GKV-X code [13],[14]. GKV-X is a nonlinear gyrokinetic Vlasov flux-tube code to perform turbulent transport simulations. The 3-D geometrical effect from magnetic configuration is included for the analysis of helical plasmas. The field aligned coordinate in the real space is used for calculations, and geometrical information of the flux surfaces is constructed by using MHD equilibrium code VMEC [17]. The nonlinear gyrokinetic equation [13],[18] for the ion perturbed gyrocenter distribution function is solved for ITG modes in the low-β electrostatic limit. The adiabatic condition is used, so the electron density and the electrostatic potential are connected with the Boltzmann relation. We want to identify the geometrical distribution of the turbulence in the 3-D magnetic configuration at first, so the electrostatic version of the gyrokinetic code with adiabatic electrons is used to produce turbulent data. The analyses are carried out using simulation data with the same parameters for ITG turbulence in the LHD high-Ti discharge in Ref. [14]; e.g., $\rho = 0.65$, $T_i = 2.2$ [keV], $n_i = 1.3\times10^{19}$ [m^{-3}], $n_i / n_e = 1$, $T_i / T_e = 1$,gradient length $L_{Ti} = 0.31$ [m], $L_n = -4.2$ [m], major radius $R_0 = 3.75$ [m], safety factor $q = 1.7$, number of simulation grids 128×128×512 and size of simulation box $98\rho_i$, $330\rho_i$, 2π (toroidal angle) in the real space (the radial, field line label, field line directions, respectively), where $\rho_i = 1.8 \times 10^{-3}$ [m] is the Larmor radius and the field line is labeled by $\alpha_L = \zeta - q\theta$ with poloidal angle θ and toroidal angle ζ. After the initial linear growth phase, the fluctuation amplitude becomes large in the nonlinear phase, where the following synthetic diagnostic is applied. Figure 1 shows the 2-D

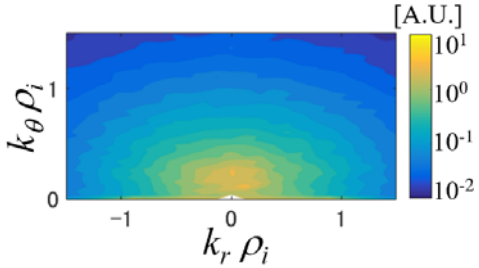

FIG 1. 2-D spectrum in the nonlinear phase in the simulation space $k_r - k_\theta$.

spectrum in the nonlinear phase in the simulation space $k_r - k_\theta$. The spectrum is anisotropic and is rather broader in k_r.

2.2.Numerical observation with line integration

We have developed an analysis routine for the GKV-X data taking into account of a LS of experimental diagnostics [15], such as PCI [19]. The PCI is used for the measurement of density fluctuation with high temporal and wavenumber k resolutions [3]. The signals are given as the integral of the density fluctuations along the LS. For the synthetic diagnostic using the simulation data, the fluctuations between incident and detector positions are depicted with the observation region size $w_1 \times w_2$, where w_1 and w_2 are the width of the observation region in the y and x directions, respectively. Here in the Cartesian coordinate $\{x, y, z\}$, z represents the direction along the LS, y represents the direction perpendicular to the z direction and on the plane parallel to the mid-plane, and x represents the direction perpendicular both to the y and z directions. The numbers of the detection points with equal intervals are set in the widths of w_1 and w_2. The geometrical configuration is the main target, so the detailed propagation and scatted process of the laser is not taken into account.

With the flux-tube configuration, regions with a finite radial width near one flux surface are taken into account. A set from a single flux-tube is used to cover whole of one flux surface by assuming the periodicity. Figure 2 shows a density fluctuation pattern constructed by this process. Figure 2 also shows the LS (A) for the numerical diagnostic, which views near the magnetic axis and is perpendicular to the mid-plane. Fluctuation data exist only in some plasma volume with a finite radial width, and there is no fluctuation in the other radial region from a single set of the flux-tube data. The GKV-X code uses the field aligned coordinate $\{x_G, y_G, z_G\}$, where coordinates x_G, z_G and y_G correspond to the directions along the minor radius, the field line and with the variation of the field line label, respectively, and calculated quantities are aligned in this coordinate. For the numerical measurement usage of the Cartesian coordinate is convenient, so interpolation is necessary for evaluating the physical quantities in the real space. Time evolutions of fluctuations are calculated in the turbulence simulation, and the temporal average of the k spectrum is taken for the nonlinear saturation phase. Improvement of the numerical PCI scheme enables to compare signals from several LSs in a helical plasma.

The obtained signal includes components perpendicular to the LS, so is usually combination of the radial and poloidal components. If the fluctuation is anisotropic, the observed signal depends on the selection of the LS. Figure 3 shows the vertical variation of the ratio of the k_r component to the k_θ component in the observation along the LS. In this case the radial components are less than 10%, so the observed components can be approximated to be the poloidal one. To obtain k spectrum a finite region around the LS is picked out, and the quantities in it are evaluated with a finite spatial resolution, corresponding to the experimental diagnostic. The width and mesh size of the region determine the resolvable k range (resolution

in the *k* space). In simulations, the observation region can be expanded to satisfy the desirable condition, so comparison with different selections of observation conditions is possible to evaluate the sufficient condition to resolve the target fluctuations. The density patterns are calculated, and the *k* spectrum is obtained with Fourier transform with the Hanning window function. The line integration and temporal average gives the 2-D *k* spectrum from the flux-tube data (Fig. 4).

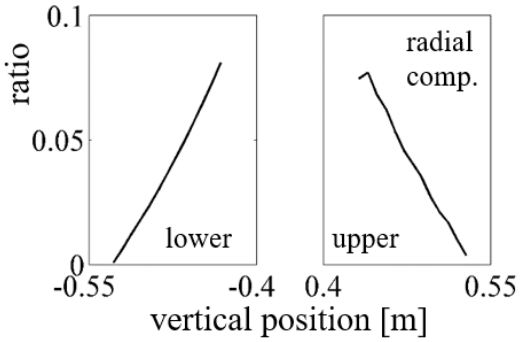

FIG 3. Vertical variation of the $\vec{k}$ component in Fig. 2. The ratio of the k_r component to the k_θ component in the observation along the LS is shown, where the simulation data exist.

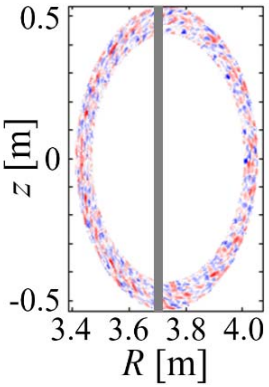

FIG 2. Snapshot of fluctuation profiles in the poloidal cross-section from GKV-X gyrokinetic simulation at ρ = 0.65. The LS is also indicated by the gray bold line.

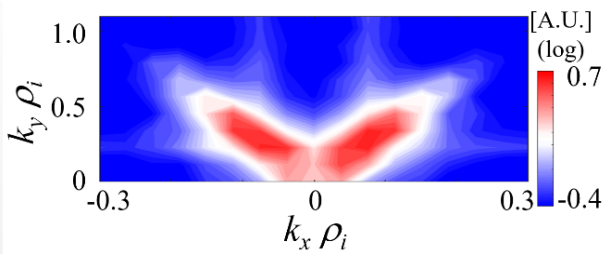

FIG4. Line integrated 2-D k spectrum from GKV-X gyrokinetic simulation at ρ = 0.65 with w_1 = 0.1[m], w_2 = 0.3[m].

2.3.Signal processing technique to improve the resolution

For the 2-D PCI, one way to improve the spatial resolution is to apply the effective conversion methods, such as the auto-regression (AR) method and the maximum entropy method (MEM) [4]. In the experimental conditions in LHD, the observation region is expected to include roughly more than one wavelength of the typical fluctuations, where the simple Fourier transform can give not so better resolution. The typical correlation pattern is obtained by averaging the cross-correlations in all the detection points with the assumption that the correlation pattern is uniform in the observation space. For improving the evaluation with a finite spatial resolution, the observation region is expanded by using models. Two methods are tested on the simulation data; (i) AR and (ii) MEM. For AR, the AR coefficients are obtained by using the Yule-Walker method. For MEM, the expansion is carried out to maximize the Burg entropy $H = \int \log S(k)\, dk$ with correlation matching, where $S(k)$ is the power spectrum. The signal processing methods can improve to give a spatial resolution 2 times better in the experiment [4], and application of the method on the simulation data confirms the possibility to identify the characteristic spectrum, wavelength and frequency in the same way (Fig. 5).

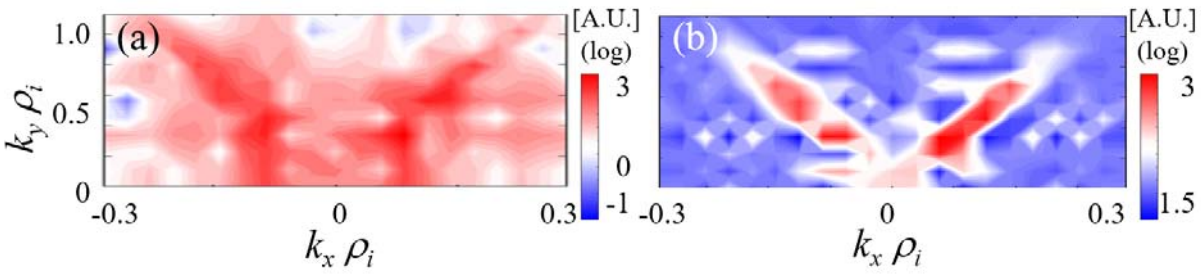

FIG5. 2-D k spectrum of the density fluctuations with (a) AR and (b) MEM.

3. Reconstruction of the local fluctuation spectrum

As the obtained signal from PCI is the line integrated one, so there is a problem to resolve the local values from the signal. The pitch angle of the magnetic field is used to help the identification [3]. The method to resolve the local spectrum from the integrated signal (2-D PCI) is applied using the simulation data [15]. ITG modes have longer wavelengths in the direction of the magnetic field, so there are characteristic k_x - k_y relation in accordance with the magnetic field direction, as in Fig. 4. Note that components with finite k along the LS become weak by the line integration, which reduces the contained components in the obtained signal. Therefore the observation is restricted to the fluctuation components along the direction, which is given by the line of intersection between the x-y and r-θ planes. The typical k direction changes in accordance with the vertical position in helical plasmas. A vertical profile of the $|k_\perp|$ spectrum can be obtained by extracting the components from the integrated signal. The vertical profile in Fig. 6 is obtained from the FFT case in Fig. 4. The original target fluctuations exist at the limited radial range indicated by the dashed rectangles, but the reconstructed profile spreads in the wider region, as shown in Fig. 6 (a). The fluctuation amplitude at each vertical position z is calculated by integration of the spectrum in k as $I(z) = \int \tilde{n}(k,z)\,dk$ (Fig. 6 (b)). There are several causes for the broadening. The large part of the leakage comes from the finite resolution due to discreteness of the data. The resolution is limited to the mesh size in the k space by the discrete Fourier transform. For the decomposition using the magnetic shear, the mesh is sparser with smaller k, so the spatial resolution is worse with smaller k as evaluated: $\Delta z \sim 0.2$ at $k\rho_i = 0.1$, $\Delta z \sim 0.1$ at $k\rho_i = 0.4$ in the observation at $z = 0.6$. The variation of the magnetic field direction in the region to calculate the spectrum gives other cause for the errors, whose contribution is comparable to the former one. The fluctuation spectrum in local positions is originally broadened to include nonzero $k_{//}$ components, which is also one of the causes for the deterioration. The local spectrum must be discussed with careful consideration of the spatial resolution.

The data produced with a flux-tube has a finite radial width, but only a limited region is covered with it. Combination of the calculations at different radii can expand the covered regions [15]. As the observation, all the density along the LS should be integrated, so every spectrum data are summed up with the weight of the mean density at the position. The vertical profile from single flux-tube data is monotonic, but that from the data combination has a multiple peak structure related to the fluctuation data distribution. Each contribution is

broadened and is overlapped, but it is confirmed that the typical shape of the spectrum is given with a single flux-tube data at the observation radius.

These simulation analyses can give a guideline for comparing simulation and experimental results. Figure 7 shows the comparison of the poloidal wavenumber spectrum for the density fluctuation amplitude *for* ρ *= 0.6 – 0.7* in the LHD experiment [14] and those obtained by the simulation. These amplitudes are normalized by their peak values to compare the spectrum shapes. The observed PCI signal is affected by the characteristics of each diagnostic. The response function depending on the wavenumber is given to be $T(k) = 1 - \exp\left[-(k/k_{\min})^2\right]$, where $k_{\min}$ is related to the cutoff in the experimental detection [12]. The evaluation of the effect from the laser propagation and scattering gives $k_{\min}\,\rho_i = 0.4$ in the LHD system. This effect is also taken into account to show the final synthetic PCI (sPCI) signal. The k value of the maximum amplitude becomes larger in the sPCI than shown in the simulation coordinate.

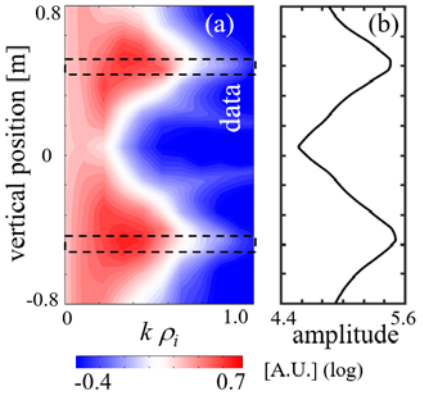

FIG 6. (a) Vertical profile of the k spectrum decomposed by using the magnetic shear method. Original simulation data exist in the region indicated by the dashed rectangles. (b)Vertical profile of the fluctuation intensity I(z) from (a).

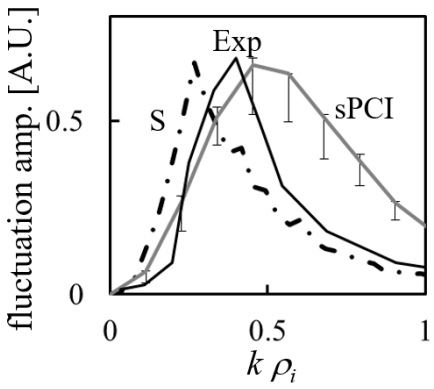

FIG 7. Poloidal wavenumber spectrum from the PCI measurement (Exp), and from the synthetic PCI (sPCI). The spectrum in the magnetic flux coordinate (S) is also shown.

4. Investigation of up-down asymmetry in numerical observation

The resolution of the diagnostic has been confirmed in the numerical observation. Even with the rough spatial resolution, quantities distant enough from each other can be identical, so the diagnostics is applied for evaluation of the up-down asymmetry.

Several factors are investigated as causes to induce the poloidal asymmetry. Here the ratio of the local fluctuation amplitude in the upper part to that in the lower part α is evaluated as the indicator for the asymmetry. The original data includes only small up-down asymmetry $\alpha \sim 1.1$, because this is given from a single flux-tube data. Firstly, (i) the effect from the 3-D magnetic configuration is evaluated. The LS in the experimental condition has a small tilt from perpendicular one to the mid-plane at the different major radius. The calculation with the experimental LS gives $\alpha = 1.2$ (Fig. 8 (a)). Secondly, (ii) the effect of some signal processing techniques explained in Subsec. 2.3 is evaluated. Figures 8 (b) and (c) show the spectra obtained with AR and MEM, respectively. It has a tendency to increase the asymmetry ($\alpha = 1.4$ and 1.8). Note that combination of effect (i) and (ii) does not always increase the asymmetry as in Fig. 8 (d) ($\alpha = 1.3$). Figure 8 (e) shows comparison of the

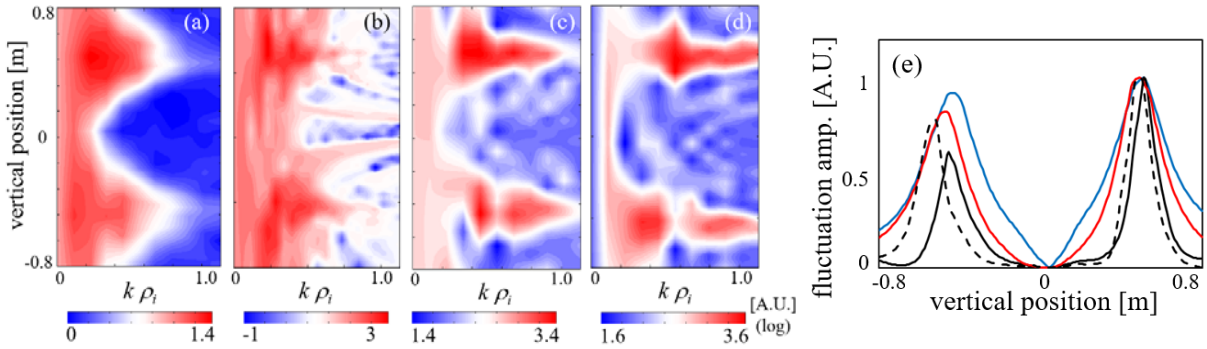

FIG. 8 Vertical profiles of the k spectrum with (a) inclusion of the experimental LS, (b) AR, (c) MEM, and (d) combination of experimental LS and MEM. (e) Comparison of the vertical profiles of fluctuation amplitudes; blue: original, red: (a), black: (c), dashed line (d).

vertical profiles of the fluctuation amplitude in (a,c,d).

(iii) The turbulent itself can have asymmetry. In helical plasmas, there is inhomogeneity both in the poloidal and toroidal directions. The flux tube simulation calculates principally local quantities, and the dependency of the instabilities on selection of the origin of the flux tube is investigated. In the LHD configuration, the toroidal dependency is rather weak, and the linear growthrate of the most unstable mode varies less than 5 %. In the poloidal direction, the linear growthrate is about 3 times larger at the low field side $\theta = 0$ than at the upper and lower parts $\theta = \pm\pi/2$. This ballooning feature is up-down symmetric. The dependence on the field line label along LS (A) is investigated by nonlinear simulations and the sPCI. Figure 9 shows the vertical profiles from the corresponding simulations. The asymmetry in the numerical observation gives $\alpha \sim 1.2$.

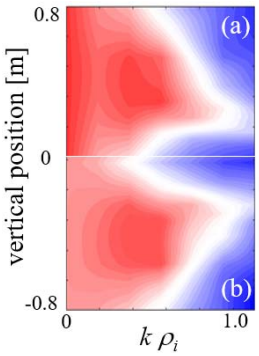

FIG. 9 Vertical profiles of the k spectrum by the simulations with the flux tube at the (a) upper and (b) lower parts of LS (A).

The effects (i)-(iii) generate the asymmetry, but is not so large (less than several tens of percent) with ITG turbulence in the LHD realistic configuration. The high-T_i discharges observing the ITG instabilities show the same level of ratio α [20],[21]. On the other hand, there is the duration in the experiment, when α becomes more than 3 [4]. Artificial reduction of the fluctuation amplitude to be half of the original value only in the bottom half of the region can give asymmetry with $\alpha \sim 3$. This implies that other causes in the turbulence must be taken into account to give the comparable asymmetry, whose origin is still unknown. The target in this paper is the case only for unstable ITG modes with considering adiabatic electrons without mean flows. The effect of kinetic electrons is not negligible, and simulations using the GKV code to consider trapped electron modes are now on going in the real magnetic geometry. Existence of the shear flow is also possible to affect the turbulence.

5. Summary

We have carried out numerical diagnostics using 3-D simulation data of the helical plasma. Gyrokinetic simulation data in the real 3-D geometry is analyzed to show the line-integrated spectrum along the LS as in experimental measurements by PCI. The pitch angle of the

magnetic field is used to reconstruct the local spectrum with consideration of a spatial resolution. In the results of the TDS application, three factors to induce the poloidal asymmetry are evaluated; 3-D magnetic configuration with the realistic LS, effect of signal processing techniques, and inherent inhomogeneity of the turbulence itself. The up-down asymmetry is rather weak for the ITG simulation as in the high-T_i regime in the experiments, where the ITG instabilities are dominant. These quantitative evaluations represent a guideline for interpretation of observed signals from experiments and simulations.

A global simulation for a long-time series with non-adiabatic electrons is still difficult due to its large computational costs in helical plasmas [22], so the combination of the multiple flux-tube simulations is tested in this research. On the other hand, a reduced fluid model with simplified magnetic configuration [23] is also useful for clarifying the detailed nonlinear mechanism of turbulent transport. It is important to integrate the results from various approaches. One of the ways for the integration is by analyzing data from the various simulations with routines to give same diagnostics as in actual experiments. Our TDS is the platform to perform such kind of analysis.

Acknowledgements

The authors acknowledge discussions with Prof. K. Itoh, Prof. S.-I. Itoh, Prof. K. Ida, Prof. S. Inagaki, Dr. M. Sasaki, and Mr. K. Kawadu. This work is supported by JSPS KAKENHI Grant Number JP24760703 and JP16K06938, by the collaboration program of NIFS (NIFS17KNST112, NIFS16KNXN323, NIFS13KOCT001) and of RIAM of Kyushu University. Some numerical simulations were carried out on "Plasma Simulator" (FUJITSU FX100) of NIFS.

References

[1] ALTUKHOV, A. B., *et al.*, Plasma Phys. Control. Fusion **58** (2016) 105004.
[2] TAKEIRI, Y., *et al.*, Nucl. Fusion **57** (2017) 102023.
[3] TANAKA, K., *et al.*, Rev. Sci. Instrum. **79** (2008) 10E702.
[4] MICHAEL, C. A., *et al.*, Rev. Sci. Instrum. **86** (2015) 093503.
[5] XANTHOPOULOS, P., *et al*, Phys. Rev. Let. 99 (2007) 035002.
[6] RHODES, T.L., *et al.*, Nucl. Fusion **51** (2011) 063022.
[7] NUNAMI, M., *et al*, Plasma Fusion Res. **6** (2011) 1403001.
[8] BAUMGAERTEL, J. A., *et al*, Phys. Plasmas **18** (2011) 122301.
[9] LIN, L., *et al.*, Phys. Plasmas **16** (2009) 012502.
[10] HOLLAND, C. *et al.*, Phys. Plasmas **16** (2009) 052301.
[11] ERNST, D. R., *et al.*, 20th IAEA FEC (Chengdu, 2006) TH1/3.
[12] ROST, J. C., LIN, L. and PORKOLAB, M., Phys. Plasmas **17** (2010) 062506.
[13] WATANABE, T. H. and SUGAMA, H., Nucl. Fusion **46** (2006) 24.
[14] NUNAMI, M., *et al.*, Phys. Plasmas **19** (2012) 042504.
[15] KASUYA, N., *et al.*, Nucl. Fusion **58** (2018) 106033.
[16] KASUYA, N., *et al.*, Plasma Fusion Res. **8** (2013) 2403070.
[17] SUZUKI, Y., *et al.*, Nucl. Fusion **46** (2006) L19.
[18] FRIEMAN, E. A. and CHEN, L., Phys. Fluids **25** (1982) 502.
[19] WEISEN, H., Rev. Sci. Instrum. **59** (1988) 1544.
[20] TANAKA, K., *et al.*, Plasma Fusion Res. **5** (2010) S2053.
[21] MIKKELSEN, D. R., *et al.*, Phys. Plasmas **21** (2014) 082302.
[22] HELANDER, P., *et al.*, Nucl. Fusion **55** (2016) 053030.
[23] KASUYA, N., *et al.*, Plasmas Phys. Control. Fusion **57** (2015) 044010.